Journal of Climate Change and Space Science *(JCCaSS)* 1(1) (2025): 4
https://doi.org/10.17576/jccass.0101.2025.04

Case Study of Two Neighbouring Interplanetary Coronal Mass Ejections

Wai-Leong Teh

Space Science Centre, Institute of Climate Change, Universiti Kebangsaan Malaysia, 43600 Bangi, Selangor, Malaysia
**Corresponding author: wteh@ukm.edu.my*

Received: 30 October 2024; Accepted: 28 January 2025; Published: 31 January 2025

ABSTRACT

Two neighbouring interplanetary coronal mass ejections (ICMEs; ICME1 and ICME2) at 1 AU, separated by ~33 hours, were compared in terms of sheath properties, geoeffectiveness, and two-dimensional (2-D) geometry. These two ICMEs have a bipolar pattern in the north-south field component. ICME2 moved at a speed of ~521 km/s, faster than the preceding ICME1 at ~460 km/s. Planar magnetic structures were found in the sheath of both ICMEs. The geomagnetic index SYM-H reached a minimum at -36 nT and -86 nT for ICME1 and ICME2, respectively. More moderate geomagnetic disturbances were caused by ICME2, due to a larger southward magnetic field. The 2-D magnetic field maps, produced by the Grad-Shafranov reconstruction, show that the two ICMEs resemble a magnetic flux rope structure but their axial directions are oppositely oriented. When viewed from the Earth, ICME1 is a right-handedness flux rope while ICME2 is a left-handedness one. This result suggests that these two ICMEs are not part of one another.

Keywords: Interplanetary Coronal Mass Ejection; Planar Magnetic Structure; Grad-Shafranov Reconstructio

1. INTRODUCTION

The space weather of the Earth is influenced by transient solar activities, for example, solar flares and interplanetary coronal mass ejections (ICMEs). Solar flares are visible on the impulsive brightening in the vicinity of sunspots, producing intensive emissions of x-ray and EUV, which are harmful to the orbiting satellites and astronauts. Usually, ICMEs are accompanied by solar flares, consisting of outbursts of energetic particles from the Sun. When the ICME reaches the Earth, it may cause severe geomagnetic field disturbances/storms (e.g., Teh et al. 2015) and thus the electrical power grids on the ground would be damaged by geomagnetically induced currents (e.g., Bolduc 2002; Marshall et al. 2012).

The moving speed of ICMEs in the interplanetary medium is supersonic (> 300 km/s), thus a shock is generated at their front. A sheath region is present in the downstream of the shock, followed by the ejecta of the ICME. The sheath is a turbulent region where the plasma is compressed and heated. Commonly, planar magnetic structures (PMSs) are seen in the ICME sheath (e.g., Nagakawa 1993; Neugebauer et al. 1993; Jones et al. 1999; Jones & Balogh 2000; Palmerio et al. 2016). The remarkable feature of PMSs is that the PMS magnetic field vectors are abruptly changed in space, but their field variations are confined to a fixed plane for hours (e.g., Jones & Balogh 2000; Palmerio et al. 2016). Therefore, the average $\boldsymbol{B} \cdot \boldsymbol{n}$ vanishes for PMSs. Here $\boldsymbol{n}$ is the unit normal vector to the fixed plane. The southward B_z field of the sheath may cause geomagnetic disturbances. In the ejecta, the plasma beta, i.e., the ratio of thermal pressure to magnetic pressure, is low ($\ll 1.0$). Observational studies show that the magnetic field configuration of the ejecta can be fitted approximately by a force-free magnetic flux rope model, where the magnetic field lines are helical and the magnetic force $\boldsymbol{j} \times \boldsymbol{B} = 0$ (e.g., Burlaga 1988; Lepping et al. 1990). The magnetic field configurations of the ICMEs can be classified into two categories, namely bipolar and unipolar flux ropes (e.g., Mulligan et al. 1998; Li et al. 2011). A bipolar flux rope has a bipolar pattern in the B_z (north-south) field component, while a unipolar flux rope contains only a southward or northward B_z. The geomagnetic disturbance/storm resulting from the ring current enhancement is measured using the SYM-H index (e.g., Teh et al. 2015), analogous to the Dst index. Significant geomagnetic storms are characterized by a minimum SYM-H index of less than -50 nT, with some storms, having a minimum SYM-H below -200 nT, capable of affecting global navigation and communication systems. By examining 38 significant geomagnetic storms caused by

the ICMEs, Teh et al. (2015) found that the minimum SYM-H was regulated by the southward B_z, regardless of bipolar or unipolar B_z, and that the axial orientations of the ICMEs had no significant relationship with the geoeffectiveness.

This paper presents a case study of two neighbouring and oppositely oriented ICMEs with a bipolar B_z. These two ICMEs are compared in terms of sheath properties, geoeffectiveness, and 2-D geometry, where the PMS analysis and the Grad-Shafranov reconstruction method are utilized.

2. OBSERVATIONS AND ANALYSIS RESULTS

Figure 1 shows two neighbouring ICMEs observed in the fast solar wind during April 12 – April 17, 2022. The data of magnetic fields (B_x, B_y, and B_z) and ion plasma moments (n_p, V_x, V_y, and V_z) were provided by OMNI at 1-minute resolution, which were time-shifted to the Earth's bow shock nose. For detailed OMNI data process, it refers to https://omniweb.gsfc.nasa.gov/html/HROdocum.html. Vector components were shown in the geocentric solar ecliptic (GSE) coordinates. The two neighboring ICMEs (ICME1 and ICME2), separated by ~33 hours, were marked by the vertical lines, where the magnetic field vectors have a smooth and large rotation, and their field strength is enhanced near the center of the structure. This magnetic field structure is analogous to a magnetic flux rope, which will be demonstrated in the next section. As indicated in Figure 1c, the plasma beta (β), the ratio of plasma thermal pressure to magnetic pressure, is typically low ($\ll 1.0$) for ICMEs. One can find a remarkable feature that the polarity of the B_x peak is different for the two neighboring ICMEs; one is directed to the Sun ($B_x > 0$) while the other points to the Earth ($B_x < 0$). This direction is related to the orientation of the ICME, which will be estimated in the next section. Moreover, for ICME1 and ICME2 there is a velocity V_x gradient across the ICME, namely a high (low) speed in the leading (trailing) part of the ICME (see Figure 1b). Figure 1d shows the electron pitch angle distribution (ePAD) at the energy 255 eV. In the ICMEs, counter-streaming field-aligned (0^o and 180^o PA) electrons were observed, suggesting that both ends of the ICMEs may be attached to the Sun.

The global geomagnetic field disturbances caused by the ICME1 were weak, where the minimum of SYM-H index was ~-36 nT (see Figure 2b). The minimum SYM-H occurred in the interval of the leading part of the ICME1, about 3 hours after the ICME1 encounter. The sheath region of the ICME1, enclosed by the shock front and the leading edge of the ICME1, is marked by the red horizontal bar (see Figure 2a). Weak field disturbances caused by the sheath were also detected. The sheath region was divided into two regions (R1 and R2) for PMS analysis. By using the minimum variance analysis of magnetic fields with the constraint $< B_n > = 0$ (Sonnerup & Scheible 1998), the normal vector $\boldsymbol{n}$ to the structure was estimated for the two regions (see Figure 2c). In Figure 2c, the magnetic field data points were displayed in the latitude (θ) – longitude (ϕ) diagram, where the red curve satisfies $\boldsymbol{B} \cdot \boldsymbol{n} = n_x \cos\theta \cos\phi + n_y \cos\theta \sin\phi + n_z \sin\theta = 0$. In the figure, λ_1 and λ_2 are the maximum and intermediate eigenvalues of the magnetic variance matrix (Sonnerup & Scheible 1998), respectively. The ratio $\lambda_1/\lambda_2 > 3$ indicates that a good estimation is obtained. For a PMS, the magnetic field data points are closely distributed along the red curve and have a wide longitudinal coverage ($> 90^o$) (e.g., Jone & Balogh 2000, Palmerio et al. 2016). The wide longitudinal coverage ensures that the magnetic field data are distributed broadly along the red line, rather than being clustered in a narrow ϕ range. It is concluded that R1 is a PMS, but R2 is not.

Unlike the ICME1, a moderate geomagnetic storm (minimum SYM-H = -86 nT) was observed at ~22:39 UT on April 14, 2022, about 5 hours after the ICME2 encounter (see Figure 3b). This storm is due to a larger southward B_z and its longer duration, as compared to ICME1. There was also a moderate geomagnetic storm (minimum SYM-H = -53 nT) occurred in the interval of the ICME2 sheath, denoted by the magenta horizontal bar. As shown in Figure 3c, the ICME2 sheath is classified as a PMS, where the normal vector is well-determined. The angle between the two normal vectors for the ICME2 sheath and R1 was ~132^o.

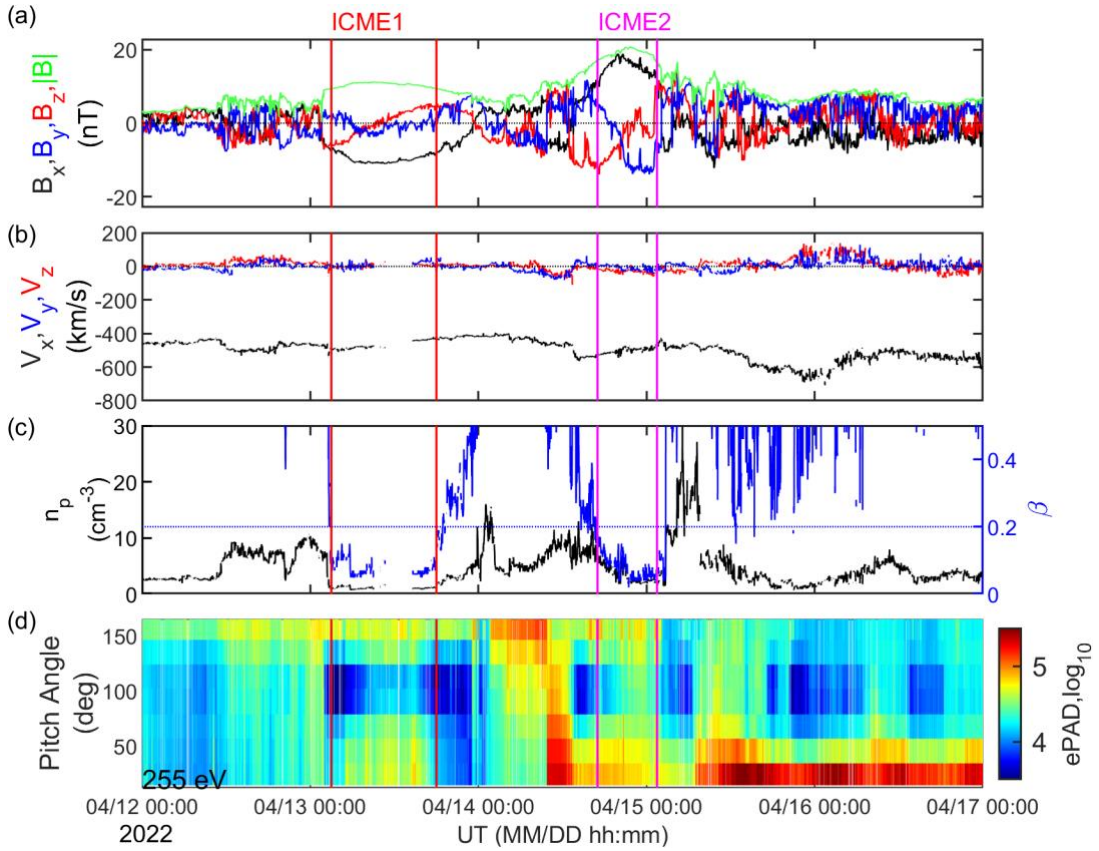

Figure 1. Observations of (a) magnetic field, (b) ion velocity, (c) ion density, and (d) electron pitch angle distribution (ePAD) for the two neighboring ICMEs in the fast solar wind. In panel (c), β is the plasma beta.

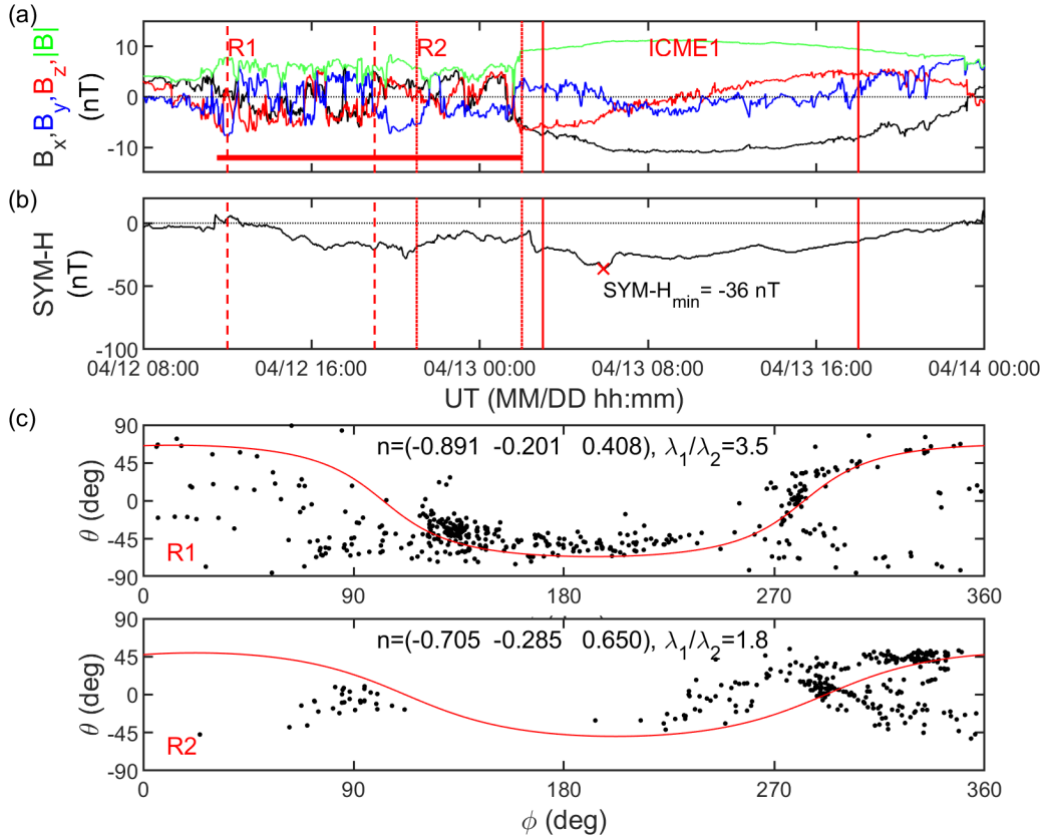

Figure 2. SYM-H measurements for ICME1 and the PMS analysis results for the sheath regions (R1 and R2).

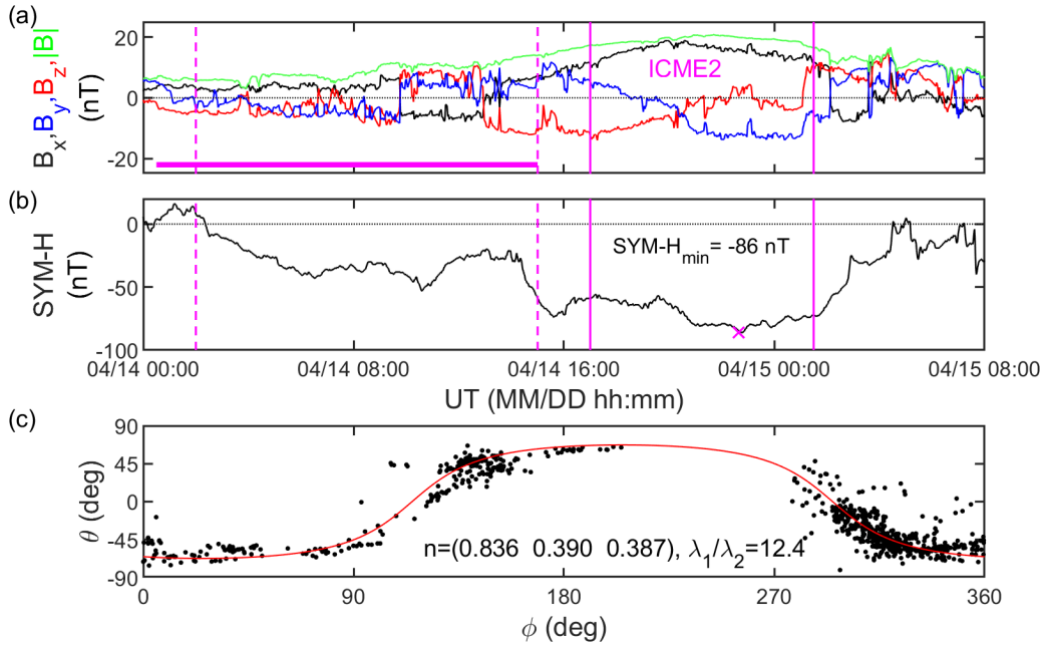

Figure 3. SYM-H measurements for ICME2 and the PMS analysis results for the sheath region enclosed by the vertical dashed lines.

3. RECONSTRUCTION OF ICME STRUCTURE

The Grad-Shafranov (GS) reconstruction scheme (Hau and Sonnerup, 1999) is implemented to reconstruct a quasi-steady ($\partial/\partial t \approx 0$), two-dimensional ($\partial/\partial z' = 0$) magnetic field configuration in the magnetohydrostatic conditions, using in-situ magnetic field and plasma measurements from a single spacecraft. This reconstruction method has been widely applied to the geometry studies of magnetic clouds and magnetic flux ropes in the solar wind (e.g., Hu and Sonnerup, 2001, 2002). Figure 4 shows the cross section of the reconstructed magnetic field lines and the axial field $B_{z'}$ in color for ICME1, for which the force-free assumption ($\boldsymbol{j} \times \boldsymbol{B} = 0$) is adopted. Here the current density $\boldsymbol{j} = \boldsymbol{\nabla} \times \boldsymbol{B}/\mu_0$. The deHoffmann-Teller frame velocity $\boldsymbol{V}_{\mathrm{HT1}}$ = (-459.4, 5.9, 14.6) km/s was used for reconstruction. It is found that ICME1 resembles a magnetic flux rope structure with right-handedness, as indicated by the green arrows (the measured magnetic fields projected onto the reconstruction plane), which rotate counterclockwise. The orientation of the ICME1 is directed along the z' axis, mainly pointing to the GSE -x axis. The reconstructed field map of the ICME2 is presented in Figure 5, with the same format as Figure 4, where the structure moved with the velocity $\boldsymbol{V}_{\mathrm{HT2}}$ = (-521.0, 2.3, -23.5) km/s. One can find that the spacecraft did not pass through the center of the flux rope, as shown in Figure 4. The orientation of the ICME2 is mainly directed along the GSE x axis, which is approximately opposite to that of ICME1 (an angle of ~168º). When viewed from the Sun, the green arrows in Figure 5 indicate a right-handedness flux rope. However, when viewed from the Earth, as for the ICME1, the ICME2 is a left-handedness flux rope.

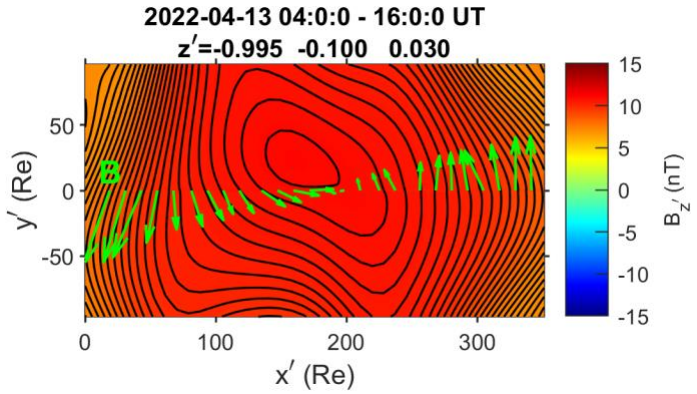

Figure 4. Reconstructed magnetic field map for ICME1. The in-plane reconstruction axes are $\boldsymbol{x}'$ = (0.100, -0.995, -0.020) and $\boldsymbol{y}'$ = (0.031, -0.017, 0.999). The green arrows are the measured magnetic fields projected on the reconstruction plane.

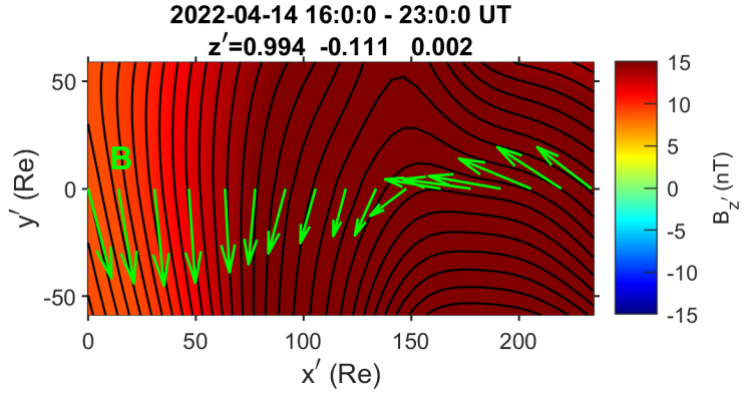

Figure 5. Reconstructed magnetic field map for ICME2. The in-plane reconstruction axes are $\boldsymbol{x}'$ = (0.102, 0.920, 0.379) and $\boldsymbol{y}'$ = (-0.044, -0.376, 0.925).

4. SUMMARY AND DISCUSSION

Two neighbouring ICMEs with a bipolar B_z (ICME1 and ICME2) at 1 AU have been compared in terms of sheath properties, geoeffectiveness, and 2-D geometry. Both ICMEs had planar magnetic structures in the sheath region. More moderate geomagnetic disturbances (minimum SYM-H = -86 nT) were caused by ICME2, due to a larger southward B_z and its longer duration. The reconstruction results indicate that the axial directions of the two ICMEs were oppositely oriented and that ICME1 is a right-handedness flux rope while ICME2 is a left-handedness one, when viewed from the Earth.

From the reconstruction maps, one can see that their field line geometry looks similar to each other, although the spacecraft did not cross the center of the ICME2. Are they part of one another? If they were, the handedness of the flux rope should not have changed when viewed from the same direction. As evident in Figures 4 and 5, when viewed from the Earth, the counterclockwise green arrows in Figure 5 become clockwise, which is opposite to those in Figure 4. Therefore, these two ICMEs are not part of one another.

Since neighboring ICMEs might lead to magnetic reconnection and thus affect solar wind dynamics, studying them can have important implications for understanding their effects on space weather and geomagnetic disturbances.

5. REFERENCES

Burlaga, L.F. (1988). Magnetic clouds: Constant alpha force-free configurations. *Journal of Geophysical Research: Space Physics*, 93, 7217.

Bolduc, L. (2002). GIC observations and studies in the Hydro-Québec power system. *Journal of Atmospheric and Solar-Terrestrial Physics*, 64(16), 1793.

Hau, L.-N. & Sonnerup, B. U. Ö. (1999). Two-dimensional coherent structures in the magnetopause: Recovery of static equilibria from single-spacecraft data. *Journal of Geophysical Research*, 104, 6899.
Hu, Q. & Sonnerup, B. U. Ö. (2001). Reconstruction of magnetic flux ropes in the solar wind. *Geophysical Research Letters*, 28, 467.
Hu, Q. & Sonnerup, B. U. Ö. (2002). Reconstruction of magnetic clouds in the solar wind: Orientations and configurations. *Journal of Geophysical Research: Space Physics*, 107, 1142.
Jones, G. H., Balogh, A., & Horbury, T. S. (1999). Observations of heliospheric planar and offset-planar magnetic structures. *Geophysical Research Letters*, 26(1), 13.
Jones, G. H., & Balogh, A. (2000). Context and heliographic dependence of heliospheric planar magnetic structurez. *Journal of Geophysical Research: Space Physics*, 105, 12713.
Lepping, R. P., Jones, J. A., & Burlaga, L. F. (1990). Magnetic field structure of interplanetary clouds at 1 AU. *Journal of Geophysical Research: Space Physics*, 95, 11957.
Li, Y., Luhmann, J. G., Lynch, B. J., & Kilpua, E. K. J. (2011). Cyclic reversal of magnetic cloud poloidal field. *Solar Physics*, 270, 331.
Marshall, R. A., Dalzell, M., Waters, C. L., Goldthorpe, P., & Smith, E. A. (2012). Geomagnetically induced currents in the New Zealand power network. *Space Weather*, 10, S08003.
Mulligan, T., Russell, C. T., & Luhmann, J. G. (1998). Solar cycle evolution of the structure of magnetic clouds in the inner heliosphere. *Geophysical Research Letters*, 25, 2959.
Nakagawa, T. (1993). Solar Source of the Interplanetary Planar Magnetic Structures. *Solar Physics*, 147, 169.
Neugebauer, M., Clay, D. R., & Gosling, J. T. (1993). The origins of planar magnetic structures in the solar wind. *Journal of Geophysical Research: Space Physics*, 98, 9383.
Palmerio, E., Kilpua, E. K. J., & Savani, N. P. (2016). Planar magnetic structures in coronal mass ejection-driven sheath regions. *Annales Geophysicae*, 34, 313.
Sonnerup, B. U. Ö., & Scheible, M. (1998). in Analysis Methods for Multi-Spacecraft Data, ed. G. Paschmann & P. Daly (Noordwijk: ESA), 185-220.
Teh, W.-L., Abdullah, M., & Hasbi, A. M. (2015). Lack of relationship between geoeffectiveness and orientations of magnetic clouds with bipolar B_z and unipolar southward B_z. *Planetary and Space Science*, 115, 27.

Acknowledgments
This work was supported by the grant of Universiti Kebangsaan Malaysia (GP-K020730). The OMNI data used in this study are publicly available from the NASA CDAWeb at http://cdaweb.gsfc.nasa.gov/.